Springer

KSME

Journal of Mechanical Science and Technology 24 (11) (2010) 2197~2206
www.springerlink.com/content/1738-494x
DOI 10.1007/s12206-010-0903-5

A performance study on a direct drive hydro turbine for wave energy converter †

Young-Do Choi[1], Chang-Goo Kim[2], You-Taek Kim[3], Jung-Il Song[4] and Young-Ho Lee[5,*]

[1]*Department of Mechanical Engineering, Mokpo National University, Jeonnam, 534-729, Korea*
[2]*Department of Mechanical Engineering, Graduate School, Korea Maritime University, Busan, 606-791, Korea*
[3]*Department of Marine System Engineering, Korea Maritime University, Busan, 606-791, Korea*
[4]*School of Mechatronics, Department of Mechanical Engineering, Changwon National University, Changwon, 641-773, Korea*
[5]*Division of Mechanical and Information Engineering, Korea Maritime University, Busan, 606-791, Korea*

(Manuscript Received July 1, 2008; Revised May 6, 2010; Accepted July 14, 2010)

Abstract

Clean and renewable energy technologies using ocean energy give us non-polluting alternatives to fossil-fueled power plants as a countermeasure against global warming and growing demand for electrical energy. Among the ocean energy resources, wave power takes a growing interest because of its enormous amount of potential energy in the world. Therefore, various types of wave power systems to capture the energy of ocean waves have been developed. However, a suitable turbine type is not yet normalized because of relatively low efficiency of the turbine systems. The purpose of this study is to investigate the performance of a newly developed direct drive hydro turbine (DDT), which will be built in a caisson for a wave power plant. Experiment and CFD analysis are conducted to clarify the turbine performance and internal flow characteristics. The results show that the DDT obtains fairly good turbine efficiency in cases with and without wave conditions. Most of the output power is generated at the runner passage of Stage 2. Relatively larger amount of the decreased tangential velocity at Stage 2 produces more angular momentum than that at Stage 1 and thus, the larger angular momentum at the Stage 2 makes a greater contribution to the generation of total output power in comparison with that at Stage 1. Large vortex existing in the upper-left region of the runner passage forms a large recirculation region in the runner passage, and the recirculating flow consumes the output power at Region 2.

Keywords: Direct drive hydro turbine (DDT); Internal flow; Performance; Wave condition; Wave power

1. Introduction

Clean and renewable energy technologies using ocean energy give us non-polluting alternatives to fossil-fueled power plants and act as a countermeasure against global warming and growing demand for electrical energy. Among ocean energy resources, wave power takes a growing interest because of its enormous amount of potential energy in the world.

To develop wave energy, various types of wave energy converters [1-12] have been developed so far to use the energy from ocean waves. Among the converter systems, the oscillating water column (OWC) type turbine is a representative converter using air as a working fluid to rotate the runner [1-8]. However, a suitable turbine type for the OWC is not generalized yet because of relatively low efficiency and high flow induced noise by the OWC turbine systems. Therefore, the direct drive hydro turbine (DDT) type converter, which uses the water flow in the turbine passage as working fluid, has been introduced to improve the turbine performance because water flow has a higher energy density compared to that of air flow [13-16]. Therefore, this study investigates the performance of a newly developed direct drive hydro turbine (DDT) for wave energy converter.

Fig. 1 shows a schematic view of the DDT, which will be built in a caisson of a wave power plant, and the turbine operation mechanism was originally suggested by Fukutomi et al. [13]. When the water with waves enters the front guide nozzle, the wave motions change to reciprocating flow in the internal flow passage of the turbine. The reciprocating flow in the turbine passage rotates the runner and thus generates output power. The runner in the turbine is designed to maintain unidirectional rotation even in the case of reciprocating flow in the turbine passage.

The shape of the front and rear nozzles has the key importance of unidirectionality of the rotor rotational direction. The flow moves bidirectionally according to the wave movements. However, the turbine rotor should be rotated in one rotational direction because only unidirectional rotation of the rotor axis can produce uniform electricity from the generator. Therefore, the shape of the front and rear nozzles has the same dimen-

† This paper was recommended for publication in revised form by Associate Editor Won-Gu Joo

*Corresponding author. Tel.: +82 51 410 4293, Fax: +82 51 403 0381
E-mail address: lyh@hhu.ac.kr

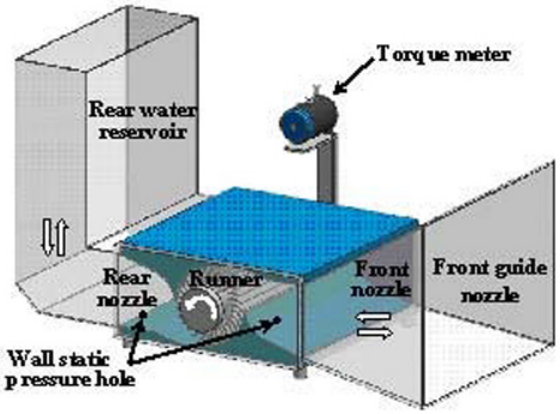

Fig. 1. Schematic view of test DDT model.

sions but is installed in the symmetric positions to the axis; the nozzles are installed at the upper wall side at front nozzle and at the bottom wall side at rear nozzle.

Even though this turbine can be applied to the wave energy converters both of the fixed and floating types, the present study is mainly focused on the application to the fixed type wave energy converter installed in a breakwater in the near-shore waters.

Experiments using a DDT model in a 2-D wave channel and numerical simulation using a commercial CFD code are carried out to investigate the performance and internal flow characteristics of the turbine.

Main purpose of CFD analysis for the basic shape of the direct drive turbine is to investigate the internal flow and performance of the turbine as well as to examine the local output power distribution according to the tangential location of the turbine rotor. Even though the present CFD analysis adopts unidirectional inflow to the turbine passage, the results by CFD analysis can explain the mechanism of output power occurrence by the inflow to the turbine. As the reverse flow to the turbine passage also causes almost the same tendency and movement of the flow field, present CFD results by unidirectional inflow can be a good reference to the actual test turbine performance by experiment with reciprocating inflow condition to the turbine passage.

2. Experimental apparatus and numerical methods

2.1 Turbine model and experimental setup

The design concept of this turbine is to apply the operation mechanism of an axisymmetric cross-flow type hydro turbine to a wave energy converter [13]. The dimensions of the test turbine are summarized as shown in Tables 1 and 2. The front guide nozzle gathers waves into the turbine and changes the waves to horizontally reciprocating flow in the turbine passage. The rear water reservoir attached to the turbine plays the role of accumulating the flow passing from the runner passage and returning the flow in contrary directions. The inflow and outflow in the turbine passage make the reciprocating flow and the flow rotates the runner in one direction constantly.

Table 1. Dimensions of test turbine for experiment.

Designed inflow velocity	v_{in}	0.43 m/s
Designed effective head	H	0.05 m
Designed rotational speed	N	45 min^{-1}
Designed output power	P_T	22 W
Turbine length		700 mm
Turbine width	b_T	700 mm
Turbine height		370 mm
Front nozzle inlet width	b_n	700 mm
Front nozzle inlet height		250 mm
Guide nozzle inlet width	b_{gn}	0.9 m
Guide nozzle inlet height		623 mm

Table 2. Dimensions of test runner for experiment.

Outer diameter	D_2	260 mm
Inner diameter	D_1	165 mm
runner width	b_T	700 mm
Outer blade angle	α	30 deg.
Inner blade angle	β	90 deg.
Blade number	Z	30

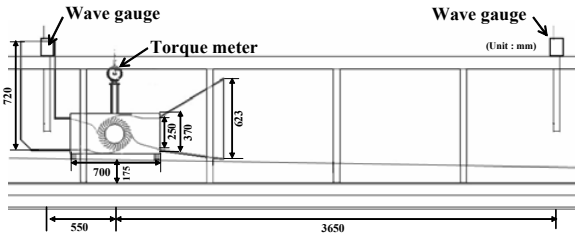

Fig. 2. Schematic view of the test facility in a 2-D wave channel.

All the experiments for the test turbine model are carried out in a 2-D wave channel as shown in Fig. 2. The wave channel has a total length of 35 m, width of 1m and depth of 1m. The bottom slope of the wave channel consists of a 7 m flat section in the deep end from a wave maker and a slope of 1:100 to the shallow end. The test turbine model is installed at the position of 15 m downstream from the wave maker in the wave channel. The piston-type wave maker, which is installed at the right end of the water channel, can generate regular waves with various wave height and wave period. By the displacement and velocity of wave paddle movements, the wave condition can be controlled. Table 3 represents the dimensions of the wave channel and the test wave condition.

Measurement instruments used in this study are summarized in Table 4. A torque meter is installed outside of the turbine and the output torque generated at the runner shaft is trans-

Table 3. Dimensions of wave channel and wave condition.

Total length		35 m
Width		1 m
Height		1 m
Bottom slope ratio		1:100
Turbine location from wave maker		15 m
Water depth	h	75 cm
Wave height	H_w	20 cm
Wave length	L	4.75 m
Wave period	T_w	2 sec.
Wave type		Regular

Table 4. Specifications of measurement instruments.

Description	Range	Product name (Maker)
Data logger	8CH	midi LOGGER GL500A (Graphtec)
Pressure transducer	0 – 200 kPa	PSHF0002KAAG (KONICS)
Capacitance wave gauge	± 25 cm	CHT4-50 (KENEK)
3-D acoustic Doppler velocimeter	0 – 7 m/s	Vector Velocimeter (NORTEC AS)
Torque meter	0 – 50 N·m	YDRM-5KM (SETech)
Revolution counter	0 - 1,000 min^{-1}	MP-981 (ONO SOKKI)
Air tension brake	0 – 20 N·m	HDB-03 (Hyundai Clutch)

ferred to the torque meter by a timing belt and a pulley. Rotational speed of the test runner is measured using a revolution counter which is attached to the torque meter. An air tension brake is used to control the rotational speed. Two pressure transducers are connected to the holes on the sidewalls both of the front and rear turbine nozzles to measure the differential pressure between the front and rear turbine nozzles. Two capacitance wave gauges are located in the water channel at the positions of 3,650 mm upstream and 550 mm downstream from the test turbine center.

The measured wave data by the wave gauge at the position upstream from the turbine guide nozzle is used for the examination of incoming wave condition, but the wave data measured at the rear water reservoir is used for determining the incoming flow rate by averaging the time serial wave height in the reservoir.

For the accurate measurement of the output torque generated in the turbine, verification of the mechanical loss caused by bearings and seals installed in the turbine is necessary because the mechanical loss occurring from relatively small rotating

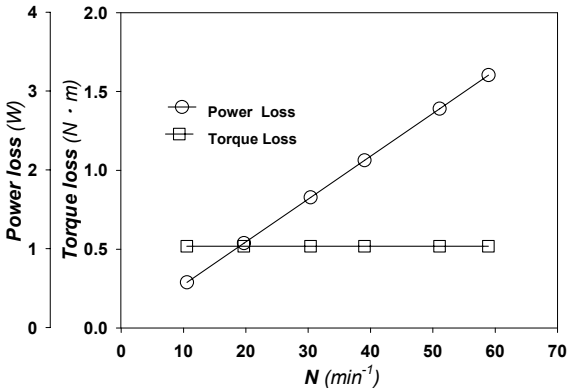

Fig. 3. Verification of mechanical loss.

machinery occupies considerable portion to the total output power loss. Therefore, this study has conducted verification test for the mechanical loss with the variation of rotational speed and the test results are floated in Fig. 3.

The measurement method of power loss and torque loss is carried out by measuring the output torque from the turbine axis when the turbine is operated under the condition of no water flow in the turbine by some constant rotational speeds. If there exists output torque without no water flow in the turbine, the output torque is definitely caused by mechanical loss. Power loss can be achieved by multiplying the torque loss and angular speed.

The measured torque loss by rotational speed is almost linear, and the measured output power loss is gradually increasing by the increase of rotational speed. The value of the output power loss is remarkable compared with the designed output power (22 W). Hence, in this study, consumed output power by the mechanical loss is restored to the total output power in order to examine the net output power generated hydrodynamically by the present DDT.

The uncertainty estimates for each variable in the graphs are based on the method of Abernethy et al. [7]. The total uncertainty (U) of the variables can be found by combining systematic and random errors as : $U = [B^2 + (tS_{\overline{X}})^2]^{1/2}$, where B is the systematic uncertainty, $S_{\overline{X}}$ is the standard deviation of the mean, and the degree of freedom t is determined to 2 for a 95% confidence level (for a sample size greater than 50). The systematic uncertainty B is estimated based on the calibration data and previous test experience, and the standard deviation of the mean $S_{\overline{X}}$ is computed from the raw test data.

Measurement uncertainties for turbine performance under a loaded condition are estimated to be Q = ± 1.39 percent, H_w = ± 1.0 percent, T_w = ± 1.4, P_T = ± 1.5 percent and h = ± 2.23 percent at the rotational speed of best efficiency, respectively.

2.2 Numerical methods

As the DDT will be installed in the wave power plant located at the offshore or nearshore waters, the performance of the turbine will be influenced considerably by the wave condi-

Table 5. Dimensions of test turbine for CFD analysis.

Designed inflow velocity	v_{in}	1 m/s
Designed Effective head	H	0.5 m
Designed rotational speed	N	45 min^{-1}
Designed output power	P_T	500 W
Turbine nozzle width	b_T	450 mm
Turbine nozzle inlet height		400 mm
Runner outer diameter	D_2	450 mm
Runner inner diameter	D_1	293 mm
Runner outer blade angle	α	30 deg.
Runner inner blade angle	β	90 deg.
Blade number	Z	26

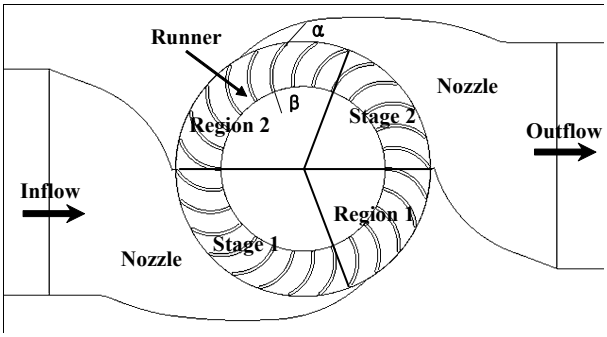

Fig. 4. Calculation domain of the turbine and division of runner passage.

tions such as wave height, wave period and the ratio of wave height vs. water depth. However, when the turbine is designed for an expected installation site, the averaged turbine performance at the design point is very important even though the turbine performance varies largely by the wave conditions. Therefore, examination of the turbine performance by the operating conditions of no-wave conditions, such as unidirectional inflow, constant flow rate and constant effective head, is necessary. For the detailed investigation of the performance and internal flow of the DDT, a 3-D finite volumetric method based commercial CFD code of ANSYS-CFX [18] is adopted and the code is well known for the excellence of analyzing the performance of turbomachinery.

Fig. 4 shows the calculation domain of the turbine. The shapes of the runner and nozzle of the turbine in Fig. 4 are same as that in Fig. 2, but the dimensions of the turbine are different. In case of the determination of the turbine nozzle shape, previous related study result by Choi et al. [19] is referred. The criterion of dividing the runner passage into the local stages and regions is determined by the zone of mainstream passage. The stage stands for a flow passage of main stream but the region represents a stagnated flow zone.

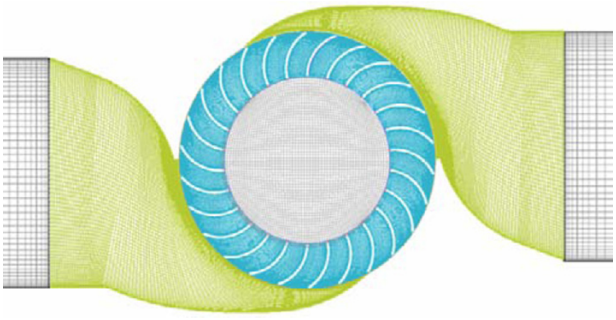

Fig. 5. Numerical grids of the turbine model for CFD analysis.

Table 5 indicates the dimensions of the test turbine for CFD analysis. The dimensions of the test turbine for CFD analysis are different from those of the test turbine for experiment (refer to Table 1). As the basic shape of the test turbine for CFD analysis could not be realized for the test turbine model for experiment in water channel, design parameters of the test turbine model for experiment are determined differently according to the turbine design method.

Numerical grids of about 1.5×10^6 are adopted for the analysis of the calculation domain including the runner and nozzle as shown in Fig. 5. Fine hexahedral grids are employed at the whole flow field to ensure the high accuracy of calculated results. To check the dependence of grid quality on the CFD result, Choi et al. [20] have investigated the turbine performance using the results from the CFD analysis by various values of dimensionless wall distance, y^+, in the calculation domains of runner and nozzle. As the calculated results for the dependence of y^+ on the turbine performance hardly show large difference under the range of $y^+ \leqq 50$, the dimensionless wall distance is kept both below 15 and below 50 in the grid regions of runner and nozzle passages, respectively.

Moreover, the dependency of three turbulence models including *SST* turbulence model has been compared using a basic DDT model from the previous related study [20]. According to the study result, *SST* turbulence model showed no large difference from the other turbulence models. However, the *SST* turbulence model has relatively good advantages of realizing both high and low energy areas simultaneously in a complicated flow field with relatively low grid dependency. Therefore, this study adopts the *SST* turbulence model.

As the boundary conditions of CFD analysis for the turbine flow field, constant pressure at the inlet and averaged flow rate at the outlet, no slip conditions on the passage walls of the calculation domain are used. Several rotational speeds are adopted for the CFD analysis to examine the turbine performance at optimum rotational speed. Moreover, the interface between the rotating parts and stationary parts for steady calculations is treated using the frozen rotor method of the adopted commercial CFD code of ANSYS CFX [18]. All the calculations are conducted under the conditions of unidirectional flow and steady state.

3. Results and discussions

3.1 Performance curves and internal flow of the DDT unidirectional steady flow

3.1.1 Performance curves and output power

Fig. 6 reveals the performance curves of the turbine model by CFD analysis under the condition of unidirectional steady flow. The performance curves result from the calculation conditions that constant pressure at the inlet and averaged flow rate at the outlet, no slip conditions on the passage walls of the calculation domain. Several rotational speeds are adopted for the CFD analysis to examine the turbine performance at optimum rotational speed. The abscissa means rotational speed N, and the ordinate indicates the efficiency η_T, output power P_T and effective head H.

The turbine efficiency η_T is given by the following equation :

$$\eta_T = \frac{P_T}{P_w} = \frac{T\omega}{\rho g Q H} \quad . \tag{1}$$

As the rotational speed increases, effective head H , which is calculated from the differential pressure between the measuring points at the front and rear nozzles of the turbine, increases almost proportionately with a steep slope. Output power P_T increases steeply by the increase of rotational speed but decreases at the range of $N > 90$ min^{-1}. In case of efficiency, after a steep increase of the efficiency until the rotational speed of N=40min^{-1}, the slope of the efficiency curve becomes gentle and the efficiency curve decreases gradually by the increase of rotational speed. Best efficiency reaches to 51.7% at the rotational speed of N = 50 min^{-1}.

The result implies that as available effective head H by wave height in an actual ocean environment can't be obtained enough to give remarkable effect on the turbine efficiency, rotational speed and incoming water flow rate should be increased to generate an optimum output power. However, as the rotational speed is restricted by the structural condition of the turbine runner, the cross-sectional area of the turbine inlet is designed as wide as possible to receive enough water flow rate for a required output power.

To investigate the output power obtained at the runner, total output power and the local output powers, which are calculated at each stage and region as defined in Fig. 4, are compared with each other as shown in Fig. 7. In case of cross-flow hydro turbine for hydro power generation, Stage 1 produces about 70% of output power and about 30% of output power is obtained at Stage 2 [21, 22]. However, the present study reveals that output powers of 16.8% at the Stage 1 and 78.1% at the Stage 2 are generated, respectively. In addition, 0.9% of the output power is consumed at the Region 2. It is conjectured that the unique proportion of the output power might be resulting from the shape of the present DDT nozzle, which is axisymmetric each other at the front and rear nozzles. Therefore, the flow passing through the runner passage is strongly

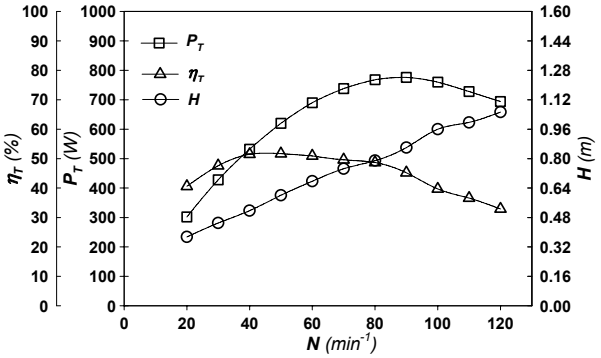

Fig. 6. Performance curves by CFD analysis.

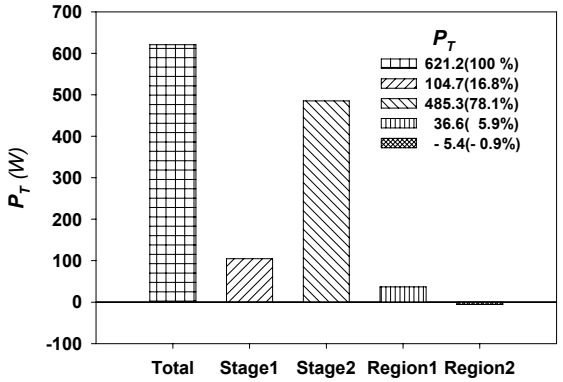

Fig. 7. Output power by CFD analysis at the best efficiency point (N=50 min^{-1}).

controlled by the unique shape of the nozzle passage and the local output powers are governed by the nozzle shape as well.

3.1.2 Velocity vectors and distributions

To examine the relation between the performance and internal flow, velocity vectors in the turbine internal passage and averaged velocity distributions at the runner blade passage are examined as shown in Fig. 8.

Fig. 8(a) shows velocity vectors in the internal flow field of the turbine model. Except for the relative velocity vectors in the runner blade passage, absolute velocity vectors are shown in the other flow passages. It is clear that flow velocity becomes accelerated within the runner center region after passing through Stage 1, and then the flow enters the runner blade passage at the Stage 2 with higher velocity than that at Stage 1. A large vortex exists at the upper-left zone of the runner internal passage and the vortex forms a wide recirculating flow within the runner passage. The recirculating flow region gives considerable influence on the output power of this turbine because the runner blades at the Region 2 consume the output power as indicated in Fig. 7. Moreover, there exists another large vortex at the bottom region in the rear nozzle passage.

Fig. 8(b) indicates the averaged velocity distributions, which are averaged from the whole blade passages at Stages 1 and 2

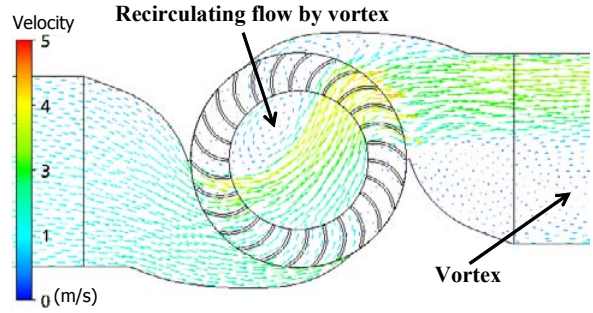

(a) Velocity vectors

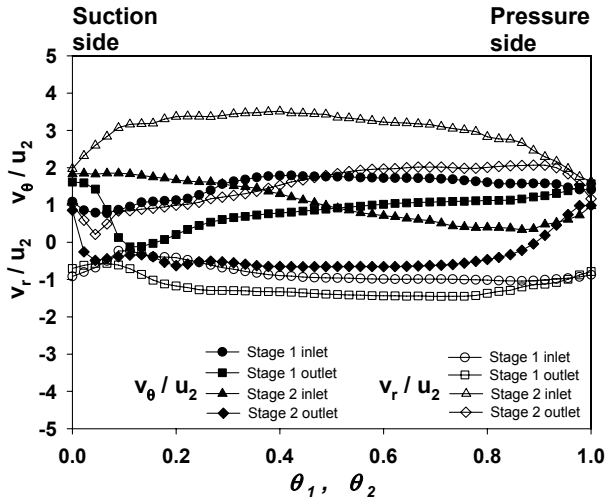

(b) Averaged velocity distribution at the runner blade passage

Fig. 8. Velocity vectors and distributions in the turbine by CFD analysis (N=50 min^{-1}).

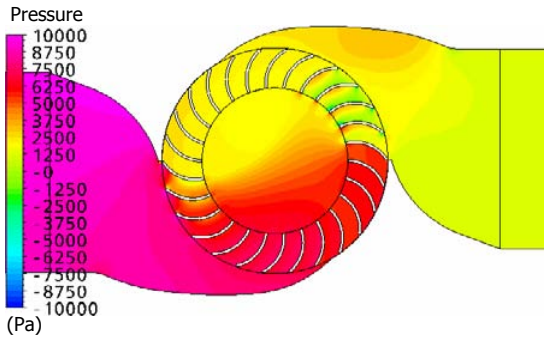

(a) Static pressure contours

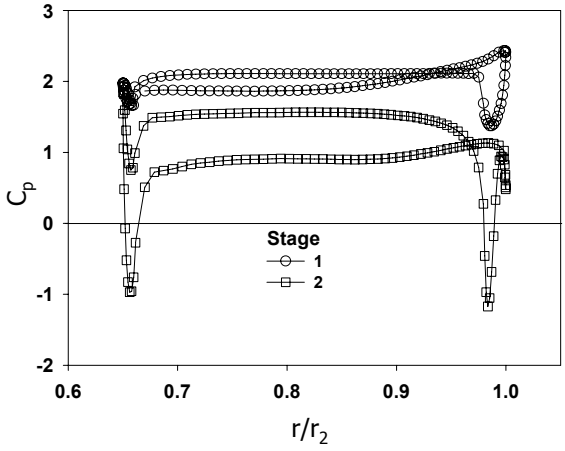

(b) Averaged pressure coefficient distribution on the surface around the runner blade

Fig. 9. Pressure contours and distributions in the turbine by CFD analysis (N=50 min^{-1}).

to the one blade passage. Tangential velocity v_θ at the inlet of Stage 1 decreases when the flow passes through the blade passage. As the flow passes through the center zone of the runner, the relatively low tangential velocity at the outlet of Stage 1 increases to the tangential velocity at the inlet of Stage 2. The tangential velocity at the inlet of Stage 2 decreases again when the flow passes through the blade passage of the stage.

While the amount of decreased tangential velocity (Δv_θ) between the inlet and outlet of the runner blade passage at the two stages is proportional to the amount of angular momentum in the runner passage ($\Delta L_{AM} = rM\Delta v_\theta$), the decreased tangential velocity between the inlet and outlet of the runner blade passage at the two stages changes to output power at the local stages. Therefore, the reason for the relatively larger output power at Stage 2 than that at Stage 1 in Fig. 7 can be explained by the present calculated result for the velocity distributions. A relatively larger amount of the decreased tangential velocity at Stage 2 produces a greater amount of angular momentum than that at Stage 1 and thus, the larger angular momentum at Stage 2 makes a greater contribution to the generation of total output power in comparison with that at Stage 1.

3.1.3 Pressure contours and pressure distributions

Fig. 9 shows static pressure contours in the turbine flow field and averaged pressure distributions on the surface around the runner blade. The static pressure contours in Fig. 9(a) show that relatively high pressure at the outlet of the turbine nozzle decreases sharply along the runner passages both at Stage 1 and Region 1. The pressures at the runner blade passage of Stage 2 and at the rear turbine nozzle are relatively very low.

Moreover, distributions of pressure coefficient by averaged pressure around the surface of the runner blades at Stages 1 and 2 are compared with each other in Fig. 9(b). The area filled with the curves of pressure coefficient means the pressure difference between pressure side and suction side of the runner blade. Therefore, a wider area filled with the pressure coefficient curve produces higher output power in the runner passage. From the result in Fig. 9(b), it is obvious that there is a wide difference between the areas by the two stages. Hence, it can be conjectured that the high tangential velocity at the inlet of Stage 2 is converted to the relatively large output power at the stage. In other words, the pressure distributions

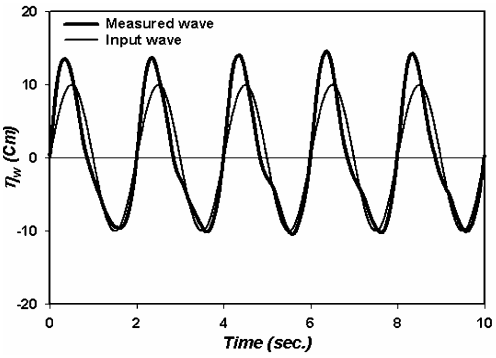

Fig. 10. Water surface elevation generated by 2-D wave maker (H_w=20 cm, T_w=2 sec., h=75 cm).

suggests that primary contribution to the output power at Stage 2 is mainly made by the effect of angular momentum acting on the surface of the runner blade at the stage.

3.2 Experimental results for test turbine performance by reciprocating flow

3.2.1 Time serial output data by the DDT

As the DDT suggested in this study will be operated in the ocean, the effect of wave conditions on the turbine performance should be considered. Therefore, a performance test is carried out with consideration for the wave conditions embodied by a regular wave maker in the 2-D wave channel.

Fig. 10 shows the wave measured at the position 3650 mm upstream from the turbine center as well as the input wave by the wave maker. The measured wave shows higher and narrower wave shape than that of the input wave at the water surface elevation η_T over 0. The transformation of the wave shape from the input wave to the measured wave is mainly influenced by the reflection wave at the inlet of the guide nozzle. The reflection wave at the guide nozzle inlet mixes with the regular wave propagated from the wave maker; then, the shape of regular wave changes to the shape of the measured wave as shown in Fig. 10.

Moreover, the measured time serial output data from the DDT model by both the no load and loaded conditions is shown in Fig. 11. Rotational speed of the runner varies regularly according to the wave movement and the averaged rotational speed N decreases from 66 to 43 min^{-1} by the applied load to the runner axis. However, as the load is applied to the turbine, outstanding increase of the instant output power $P_{T\ instant}$, instant output torque $T_{instant}$ and instant effective head $H_{instant}$ can be recognized.

3.2.2 Performance curves

Fig. 12 shows performance curves of the turbine model by the wave condition of wave height H_w=20 cm and wave period T_w=2 sec. Effective head H and flow rate Q reveal linear decrease with gentle slope by the increase of rotational speed N but output torque T decreases with steep slope at the rotational speed of $N > 43$ min^{-1}.

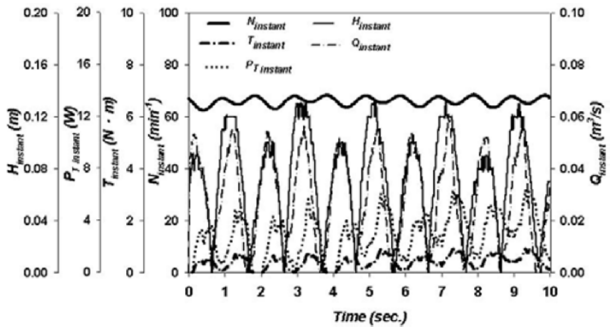

(a) No load condition (N=66 min^{-1})

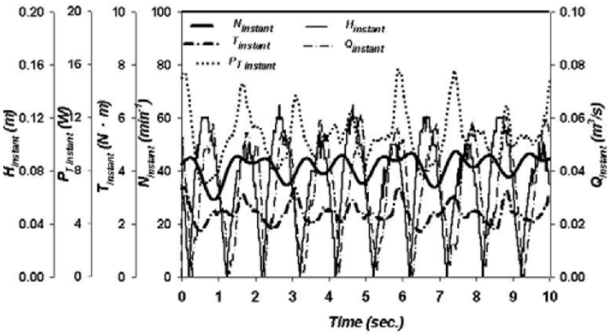

(b) Loaded condition (N=43 min^{-1})

Fig. 11. Time serial output data by the turbine (H_w=20 cm, T_w=2 sec., h=75 cm).

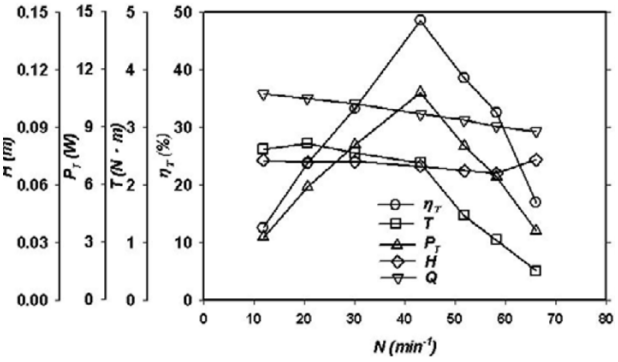

Fig. 12. Performance curves of the test turbine (H_w=20 cm, T_w=2 sec., h=75 cm).

Meanwhile, the change of the efficiency η_T and output power P_T by rotational speed shows steep increase and decrease with the turning point of a sharp peak at the rotational speed of N = 43 min^{-1}. This result implies that when the wave enters to the turbine internal passage with a certain wave height and a wave period, the effective head H and flow rate Q change little by rotational speed but best efficiency and maximum output torque occur at an optimum range of the rotational speed. Therefore, the designed point of the turbine should be determined with consideration for the wave condition at the expected installation site to achieve optimum performance during the turbine operation.

Table 6. Efficiency analysis of the turbines for wave energy converter.

Project Name	Institute (Country)	Turbine type	Place of exp.	Designed output power (P_D)	Guide nozzle width	Significant wave height ($H_{1/3}$)	Wave period ($T_{1/3}$)	Wave energy[(1)] (P_{wave} or P_{sea})	Guide nozzle efficiency (η_{gn})	Turbine efficiency (η_T)	Generator efficiency (η_G)	Total efficiency ($\eta_{overall}$)
LIMPET [5]	WaveGen (U.K.)	OWC	Water channel	-	-	-	-	-	Max. 80.0%	-	-	-
			Ocean	500 kW (250 kw×2)	20 m	-	-	12 kW/m	64.0%	40.0% (D_I=2.6 m)	-	8.7%
Mighty whale [6]	JAMSTEC (Japan)	OWC	Water channel	-	1.5 m	3 cm - 15 cm	1.0 s - 2.5 s	-	Max. 55.0%	48.0% (D_I=298 mm)	-	-
			Ocean	50 kW	30 m	1.5 m	7.0 s	-	Max. 33.0%	45.0% (D_I=1.7 m)	90.0% (estimated)	13.2%
Sakata port [7]	PARI (Japan)	OWC	Water channel	-	0.8 m	0-52 cm	1.34 s - 3.35 s	-	Max. 70.0%	-	-	-
			Ocean	60 kW	20 m	2.27 m	7.4 s	15.9 kW/m	23.1%	35.6% (D_I=1.337 mm)	92.9%	7.7%
Present study	Korea Maritime University (Korea)	DDT	Water channel	22 W	0.9 m	20 cm	2.0 s	80.68 W	27.5% (50% designed)	48.6% (D_I=260 mm) (60% designed)	90.0% (estimated)	12.03% (27.3% designed)
Remarks	(1) Reference equation for wave energy estimation : equation (2) for water channel, equation (3) for ocean											

3.2.3 Efficiency analysis of the DDT

The incoming wave motions to the DDT model change to reciprocating water flow by the guide nozzle, and the reciprocating flow in the turbine passage rotates the runner when the flow passes through the runner blade passages. Therefore, local efficiencies at the guide nozzle (η_{gn}) and the turbine model (η_T), as well as total efficiency ($\eta_{overall}$) are investigated to examine the performance of the turbine system in detail.

When a regular wave is given in the wave channel, wave power P_{wave} is calculated by the following equation [14]:

$$P_{wave} = \frac{1}{16}\rho g Q H_i^2 \frac{L}{T_w} b_{gn}\left[1+\frac{\frac{4\pi h}{L}}{\sinh\left(\frac{4\pi h}{L}\right)}\right] . \quad (2)$$

Moreover, in the case of irregular wave in the ocean, the wave power P_{sea} is given by the following equation [23]:

$$P_{sea} = \frac{\rho g^2 H_s^2 T_z}{64\pi K_{sm}^2}\times 0.001 = 0.492\frac{H_s^2 T_z}{K_{sm}^2} . \quad (3)$$

where

$$K_{sm} = \frac{1}{\sqrt{2n\tanh k_m h}},\ n=\frac{1}{2}C,\ C=\left[1+\frac{\frac{4\pi h}{L}}{\sinh\left(\frac{4\pi h}{L}\right)}\right]$$

While, total efficiency $\eta_{overall}$ of the present DDT model is calculated by the following equation:

$$\eta_{overall} = \eta_{gn}\times\eta_T\times\eta_G . \quad (4)$$

where the converting efficiency of the guide nozzle (η_{gn}) can be calculated by $\eta_{gn} = P_w / E_{total}$ in case of water channel experiment, and the incoming wave energy at the guide nozzle inlet (E_{total}) can be calculated by $E_{total} = P_{wave} \times b_{gn}$. In addition, wave energy at the ocean with irregular waves is calculated by $E_{total} = P_{sea} \times b_{gn}$.

Therefore, the efficiencies at the turbine local regions and total efficiency by the present turbine system are summarized in Table 6. For the comparison of the DDT efficiency with other types of the turbine for wave energy converters, some other research results are summarized as well. Even though the test environments for each turbine system are different, turbine efficiency of the present DDT model is remarkable compared with those of the other turbine systems. However, for greater improvement of the total efficiency $\eta_{overall}$ to the designed value, optimization for the shapes of both the guide nozzle and the turbine flow passage is necessary.

4. Conclusions

(1) The present direct drive hydro turbine system shows fairly good turbine efficiencies of 51.7% at the best point by unidirectional steady flow without input wave condition and 48.6% by reciprocating flow with an input wave condition in a 2-D wave channel. For greater improvement of total efficiency for the turbine system, optimization for the shapes of both the guide nozzle and the turbine flow passage is necessary.

(2) Most of the output power generated at the runner blade passage of the Stage 2 and the output power generated in the local runner passage reaches to 78.1% of total output power. Relatively larger amount of the decreased tangential velocity at Stage 2 produces more angular momentum than that at Stage 1 and thus, the larger angular momentum at Stage 2 makes a more contribution to the generation of total output power in comparison with that at Stage 1.

(3) A large vortex existing in the upper-left region of the runner passage forms a large recirculation region in the runner passage and the recirculating flow consumes the output power at the Region 2.

(4) Designed point of the turbine should be determined in consideration for the wave condition at the expected installation site to achieve optimum performance during the turbine operation. Among the design parameters for the test turbine, key importance is kept to the rotational speed in this study. Best efficiency is located in the adjacent of rotational speed of N=45min^{-1} as expected in the designed parameter.

Nomenclature

b_T : Width of nozzle and runner
b_{gn} : Width of guide nozzle inlet
C_p : Pressure coefficient $(=(p-p_{ref})/\rho gH)$
g : Acceleration of gravity
H : Effective head
H_i : Incoming wave height
H_s : Significant wave height
H_w : Wave height
h : Water depth
k_m : Root mean square wave number
K_{sm} : Root mean square shallow water coefficient
L : Wave length
L_{AM} : Angular momentum
M : Mass of water
N : Rotational speed
P_T : Turbine output power
P_w : Water input power
P_{wave} : Waver energy by regular wave
p : Static pressure
p_{ref} : Reference static pressure at the turbine rear nozzle
P_{sea} : Wave energy by irregular sea wave
Q : Volumetric flow rate
r : Runner radius
r_2 : Outer radius of runner
T : Output torque
T_w : Wave period
T_z : Zero up-crossing period
u_2 : Runner rotational speed at outer radius
v_r : Radial velocity
v_θ : Tangential velocity
η_T : Turbine efficiency
η_G : Generator efficiency
η_{gn} : Guide nozzle efficiency
$\eta_{overall}$: Generator efficiency
η_w : Water surface elevation
θ_1 : Normalized peripheral blade position in one blade passage at Stage 1
θ_2 : Normalized peripheral blade position in one blade passage at Stage 2
ρ : Density of water
ω : Angular velocity

References

[1] T. Setoguchi, S. Santhakumar, H. Maeda, M. Takao and K. kaneko, A review of impulse turbines for wave energy conversion, *Renewable Energy* 23 (2001) 261-292.

[2] T. Setoguchi, S. Santhakumar, M. Takao, T. H. Kim and K. Kaneko, A performance study of a radial turbine for wave energy conversion, *Proc. Instn Mech Engrs Part A : Power and Energy* 216 (1) (2002) 15-22.

[3] R. Curran, Productivity of ocean-wave energy converters : turbine design, *J. Energy Engineering* 128 (2) (2002) 13-31.

[4] D. G. Dorrell, M-F. Hsieh and W. Fillet, Segmented small oscillating water columns using in-line savonius rotors, *Proc. the 7th International Offshore and Polar Engineering Conference*, Lisbon, Portugal (2007).

[5] Research into the further development of the LIMPET shoreline wave energy plant, *Supplement to the Final Report to DTI Sustainable Energy Programme*, Wavegen, U.K. (2003).

[6] *Research and development of wave energy utilization technology - development of offshore floating type wave energy converter 「Mighty Whale」*, JAMSTEC (in Japanese), Japan (2004).

[7] S. Takahashi, T. Adachi, H. nakada, H. Ohneda, H. Katou and M. Shikamori, Field experiment of a wave power extracting caisson breakwater - data analysis of wave forces and wave power conversion, *Report of the Port and Harbour Research Institute*, 31 (2) (1992) 21-54.

[8] J-S. Moon, K-Y. Hong, S-H. Shin, B-S Hyun, H-J Ryu and S-J Park, Oscillating flow field analysis as shape of air chamber in OWC-type wave energy conversion, *J. of Korean Navigation and Port Research,* 31 (1) (2007) 29-33.

[9] J. Tedd, J. P. Kofoed, M. Jasinski, A. Morris, E. Friis-Madsen, R. Wisniewski and J. D. Bendtsen, Advanced control techniques for WEC wave dragon, *Proc. the 7th European Wave and Tidal Energy Conference*, Porto, Portugal (2007).

[10] S. J. Beatty, B. J. Buckham and P. Wild, Modeling, design and testing of a two-body heaving wave energy converter, *Proc. the 7th International Offshore and Polar Engineering Conference*, Lisbon, Portugal (2007).

[11] *Brochure of pelamis P-750 wave energy converter*, Pelamis Wave Power Ltd. (2008).

[12] M. Folley, T. J. T. Whittaker and A. Henry, The effect of water depth on the performance of a small surging wave en-

ergy converter, *Ocean Engineering* 34 (2007) 1265-1274.
[13] J. Fukutomi and Y. Nakase, A study of turbine for wave power generation, *Proc. of the 1st Pacific / Asia Offshore Mechanics Symposium*, Seoul, Korea (1990) 193-198.
[14] G. Orer and A. Ozdamar, An experimental study on the efficiency of the submerged plate wave energy converter, *Revewable Energy* 32 (2007) 1317-1327.
[15] S. Kondo, K. Taniya, K. Takahashi, H. Watabe and K. Okuda, Study on the wave energy absorption devices installed in the breakwater facility - wave power turbine type, *Proc. the 28th Coastal Engineering Conference* (in Japanese), (1981) 381-385.
[16] H. Watabe, S. Kondo, K. Taniya, E. Takeda and S. Kuroi, Study on the wave energy absorption devices installed in the breakwater facility - pendulum type, *Proc. the 29th Coastal Engineering Conference* (in Japanese), (1982) 486-490.
[17] R. B. Abernethy, R. P. Benedict and R. B. Dowdell, ASME measurement uncertainty, *ASME J. Fluids Eng.* 107 (1985) 161-164.
[18] *ANSYS-CFX Documentation Ver. 11*, ANSYS Inc. (2007).
[19] Y-D. Choi, C-G. Kim, Y-T. Kim and Y-H. Lee, A study on the nozzle shape of a cross-flow type hydro turbine for wave power generation, *J. of Fluid Machinery* (in Korean) 11 (3) (2008) 30-35.
[20] Y-D. Choi, Y-J. Cho, Y-T. Kim and Y-H. Lee, Performance and internal flow of a cross-flow type turbine for wave power generation, *J. of Fluid Machinery* 11 (3) (2008) 22-29.
[21] A. A. Fiuzat and B. P. Akerkar, Power outputs of two stages of cross-flow turbine, *J. Energy Engineering* 117 (2) (1991) 57-70.
[22] Y-D. Choi, J-I. Lim, Y-T. Kim and Y-H. Lee, Performance and internal flow characteristics of a cross-flow hydro turbine by the shapes of nozzle and runner blade, *J. of Fluid Science and Technology*, 3 (3) (2008) 398-409.
[23] H-J. Ryu, K-H. Hong, S-H. Shin and D-Y. Kim, A study on wave condition and design wave for the optimal design of wave power generator, *Proc. of Korea Ocean Science and Technology Association Conference* (in Korean), Korea (2007) 1800-1807.

Young-Do Choi received his B.E. and M.E. in Mechanical Engineering from Korea Maritime University, Korea in 1996 and 1998, respectively. He then received his Dr. Eng. degree from Yokohama National University, Japan in 2003. Dr. Choi is currently a fulltime lecturer at the Department of Mechanical Engineering, Mokpo National University in Jeonnam, Korea. His research interests include ocean energy, wind power, small hydro power, fluid machinery, PIV and CFD.

Young-Ho Lee received his B.E. and M.E. degrees from Korea Maritime University, Korea. He then received his Dr. Eng. degree from the University of Tokyo, Japan. Dr. Lee is currently a Professor at the Division of Mechanical and Information Engineering, Korea Maritime University in Busan, Korea. His research interests include ocean energy, wind energy, small hydro power, fluid machinery, PIV and CFD.